JACS
JOURNAL OF THE AMERICAN CHEMICAL SOCIETY
Article
pubs.acs.org/JACS

Molecular Lifting, Twisting, and Curling during Metal-Assisted Polycyclic Hydrocarbon Dehydrogenation

Davide Curcio,[†,#] Luca Omiciuolo,[†,#] Monica Pozzo,[‡] Paolo Lacovig,[¶] Silvano Lizzit,[¶] Naila Jabeen,[†,§,∥] Luca Petaccia,[¶] Dario Alfè,[‡] and Alessandro Baraldi*[,†,¶,⊥]

[†]Physics Department, University of Trieste, Via Valerio 2, 34127 Trieste, Italy
[‡]Department of Earth Sciences, Department of Physics and Astronomy, Thomas Young Centre@UCL, London Centre for Nanotechnology, University College London, Gower Street, London WC1E 6BT, United Kingdom
[¶]Elettra-Sincrotrone Trieste S.C.p.A., Strada Statale 14 km 163.5, 34149 Trieste, Italy
[§]International Centre for Theoretical Physics, Strada Costiera 11, 34151 Trieste, Italy
[∥]Nanosciences & Catalysis Division, National Centre for Physics, Islamabad 44000, Pakistan
[⊥]Laboratorio TASC, IOM-CNR, AREA Science Park, Strada Statale 14 km 163.5, 34149 Trieste, Italy

Supporting Information

ABSTRACT: The atomistic understanding of the dissociation mechanisms for large molecules adsorbed on surfaces is still a challenge in heterogeneous catalysis. This is especially true for polycyclic aromatic hydrocarbons, which represent an important class of organic compounds used to produce novel graphene-based architectures. Here, we show that coronene molecules adsorbed on Ir(111) undergo major conformational changes during dissociation. They first tilt upward with respect to the surface, still keeping their planar configuration, and subsequently experience a rotation, which changes the molecular axis orientation. Upon lifting, the internal C−C strain is initially relieved; as the dehydrogenation proceeds, the molecules experience a progressive increase in the average interatomic distance and gradually settle to form dome-shaped nanographene flakes. Our results provide important insight into the complex mechanism of molecular breakup, which could have implications in the synthesis of new carbon-based nanostructured materials.

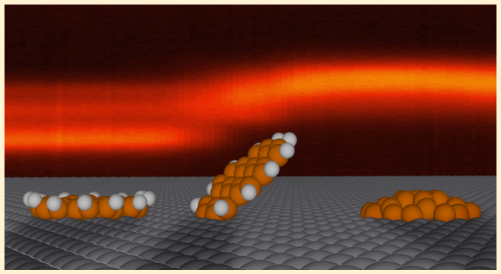

INTRODUCTION

The process of surface-assisted cyclodehydrogenation of polycyclic aromatic hydrocarbons (PAHs) has been adopted in recent years as one of the most effective, versatile, and flexible strategies for the bottom-up synthesis of fullerenes,[1] small graphene flakes (nanographene), and nanoribbons.[2−4] The large number of available precursors is the key to tailor the structural properties of low-dimensional carbon networks via polymerization reactions and to control their chemical and transport properties, which are promising for applications in optoelectronics and molecular electronics. In particular, the band gap problem in graphene can be overcome by exploiting quantum confinement effects, which allow for modification of the band gap by adjusting the width and the type of edge terminations.[5−10] However, the pathway of molecular dissociation becomes more complex with increasing molecular extension, number of sequential reaction steps, degrees of freedom for molecular motion, and competition with desorption processes. The initial-state PAH adsorption configuration, which can be influenced by intermolecular or substrate-mediated interactions, can also strongly affect the dissociation mechanism. For example, the reported thermally induced dehydrogenation of polyphenylene molecules on Cu(111)[11] proceeds via six intermediate steps of aryl−aryl coupling reactions. For polyphenylene molecules, the partial dehydrogenation of the large hydrocarbons leads to a H-terminated nanographene, although in this case, the interaction with the substrate plays only a marginal role, and the partial reaction barriers are similar for the noncatalyzed dehydrogenation. It is clear that detailed knowledge of the chemical, structural, and electronic transformations involved in each cyclodehydrogenation step is a prerequisite for finding more efficient routes to fabricate novel nanographene/nanoribbon structures with tailored properties. In this study we show that thermally assisted cyclodehydrogenation of coronene ($C_{24}H_{12}$) on Ir(111) takes place through sequential steps that include dramatic changes of the molecule's pristine configuration. For a comprehensive characterization of the reaction process, we adopted a combined theoretical and experimental approach where density functional theory (DFT) calculations accompanied the experiments performed combining several techniques, namely fast and high-energy resolution X-ray photoelectron spectroscopy (HR-XPS), near-edge X-ray absorption fine structure (NEXAFS), ultraviolet photoelectron spectroscopy (UPS), angle resolved photoemission spectroscopy

Received: November 30, 2015
Published: February 1, 2016

DOI: 10.1021/jacs.5b12504
J. Am. Chem. Soc. 2016, 138, 3395−3402

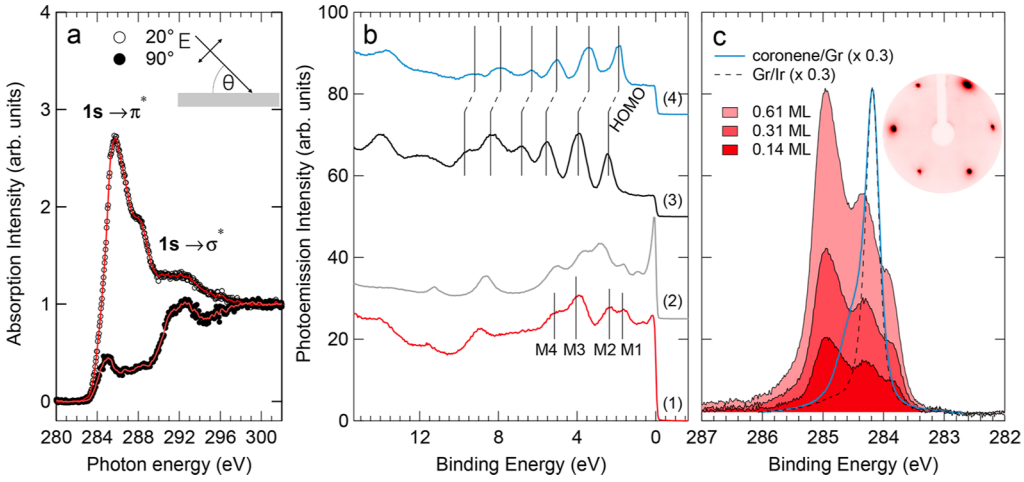

Figure 1. (a) C K-edge NEXAFS spectra for coronene/Ir(111) acquired with linearly polarized radiation, with the electric field vector either parallel (filled circles) or almost normal (open circles) to the crystal surface. (b) Valence band spectra measured at $h\nu$ = 34 eV of (1, red curve) monolayer coronene on Ir(111), (2, gray curve) clean Ir(111), (3, black curve) multilayer coronene on Ir(111), and (4, blue curve) monolayer coronene on graphene/Ir(111). Identified molecular orbitals are, right to left (black bars on spectra (3), (4)): E_{2u} first peak; B_{1g}, B_{2g}, E_{1g} second peak; E_{2u}, A_{2u}, E_{2g} third peak. Molecular orbitals M1, M2, M3, and M4 on spectrum (1), associated with nondispersing features in the ARPES maps (see Supporting Information Figure S1), have been marked with vertical lines. (c) C 1s spectra measured at $h\nu$ = 400 eV for three different coverages of coronene on Ir(111), compared with monolayer coronene on graphene/Ir(111) (blue curve) and pristine graphene on Ir(111) (dotted curve), and (inset) LEED pattern acquired at 86 eV electron energy after about 0.14 ML coronene deposition.

(ARPES), temperature-programmed desorption (TPD), and low-energy electron diffraction (LEED).

EXPERIMENTAL SECTION

The Ir(111) single crystal used in this experiment was cleaned in ultra-high-vacuum (UHV) conditions by repeated cycles of Ar^+ sputtering at 2 keV and annealing to 1400 K, followed by annealing cycles in oxygen pressure to remove any carbon contaminants. A final annealing in hydrogen atmosphere was performed to remove residual oxygen from the surface. This procedure was optimized to ensure a high-quality surface, as judged by LEED and XPS. The measurements reported in this work were performed in UHV conditions, with a base pressure of the order of 1×10^{-10} mbar.

Commercially available (Sigma-Aldrich) coronene powder (99%, purified by sublimation) was used throughout the experiment. Coronene molecules were evaporated in a vacuum using a custom evaporator consisting on a boron nitride (BN) crucible wrapped with a 1 mm diameter Ta wire used to heat it by resistive dissipation. The crucible was cleaned in a vacuum before the experiment by means of a long annealing to increasing temperatures up to 670 K, in order to clean the evaporation cell of impurities. The temperature inside the crucible was measured through a type K thermocouple in thermal contact with the coronene powder. Coronene evaporation was achieved by keeping the crucible at a fixed temperature, varying from 400 to 440 K. Before evaporation, coronene was further purified in a vacuum by means of repeated short annealing cycles up to 450 K, while the chamber residual gas composition was monitored with a residual gas analyzer system. Calibration of the coronene evaporation rate was achieved by comparing the photoelectron intensity to a reference signal acquired, with the same acquisition parameters, after graphene growth on Ir(111). On the basis of the C(10×10)/Ir(9×9) moiré unit cell observed for single-layer graphene on Ir(111), the reference coverage was assumed to be 2.47 monolayer (ML).

High-resolution (HR) and temperature-programmed (TP) XPS[12] measurements were carried out at the SuperESCA beamline of the Elettra synchrotron radiation facility (Trieste, Italy). A state-of-the-art SPECS PHOIBOS 150 hemispherical analyzer was employed, equipped with a delay line detector developed at Elettra. C 1s spectra were acquired in normal emission geometry with a photon energy of 400 eV, along with a measurement of the Fermi level on the sample, which was used to align the binding energy (BE) scale. The X-ray beam on the sample, at normal emission, measures 300 μm in the horizontal direction and 10 μm in the vertical one. In order to check for possible X-ray-induced molecular breakup, we performed several scans along the surface to search for C 1s spectral modifications, without finding appreciable differences.

NEXAFS measurements were performed at the SuperESCA beamline of Elettra. Carbon K-edge absorption spectra were acquired in the Auger electron yield configuration, with a photoelectron kinetic energy of 260 eV and a photon energy range between 280 and 315 eV. Two different angular configurations were used, corresponding to incidence angles of 0° and 70° with respect to the surface.

Valence band photoemission spectra were acquired at the BaDElPh beamline of Elettra using a state-of-the-art SPECS PHOIBOS 150 hemispherical analyzer combined with a 2D detector consisting of a phosphor screen coupled with a 2D-CCD commercial detector. The UPS spectra were measured with photon energy equal to 34 eV in a ±13° wide angular region centered in the K-point of the reciprocal space. The ARPES maps were also acquired with 34 eV photon energy.

The LEED experiments were carried out at the Surface Science Laboratory of Elettra-Sincrotrone Trieste using a VG rear-view electron optical system.

The TPD curves were acquired at the Surface Science Laboratory at Elettra using an SRS 200 residual gas analyzer. During the experiment the sample was annealed at a fixed rate of 2.5 K/s by means of three hot W filaments placed a few millimeters behind the sample.

The C 1s spectra were analyzed using a sum of 24 Doniach–Šunjić functions[13] convoluted with Gaussians, including a Shirley-type background. The relative BE shifts between the components were constrained to the ones predicted by DFT, while a rigid shift was imposed to align the experimental BE scale to the theoretical one. The Lorentzian and Gaussian widths, as well as the asymmetry parameters, were constrained to be the same for all peaks. This implicates the following assumptions: the core electronic states corresponding to the different C atoms in the molecule have the same finite lifetime (resulting in an equal Lorentzian broadening); all the core-level components are affected to the same extent by thermal phonon broadening, experimental, and inhomogeneous broadening (which are reflected in their Gaussian fwhm); and the chance of an electron–hole pair excitation event is the same for each core level (resulting in an equal asymmetry parameter). The intensities were also constrained to be equal. All experimental data and fitting results have been displayed after subtraction of the background found by the fitting operation.

DOI: 10.1021/jacs.5b12504
J. Am. Chem. Soc. 2016, 138, 3395–3402

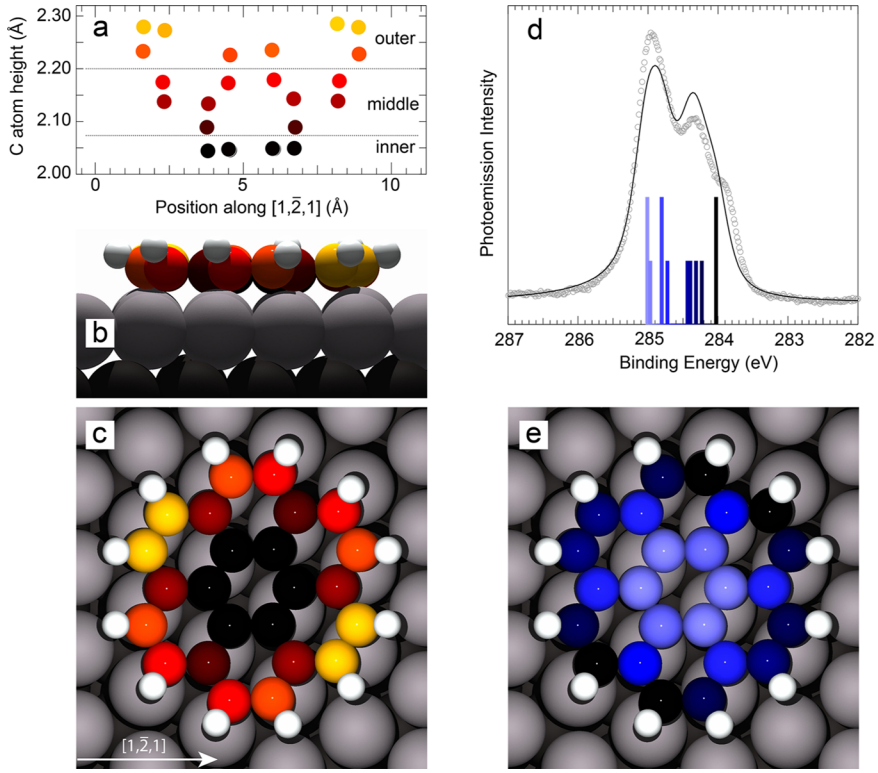

Figure 2. (a) Carbon−iridium distance for the nonequivalent C atoms of the coronene molecule. (b,c) Illustration of the side and top views of the $C_{24}H_{12}$ molecular orientation as found in DFT calculations. The color scale reflects the separation between the C atoms and the substrate beneath. Small differences in the C−Ir distance between apparently equivalent C atoms can be accounted for by considering the small influence of the second Ir layer, which breaks the 6-fold symmetry of the first atomic layer. (d) C 1s spectrum measured at normal emission and $h\nu$ = 400 eV (empty circles) together with the fit result (solid line) and the calculated spectral distribution originated from the 24 C atoms. (e) Color scale in the model reflects the BEs of the different C 1s calculated components.

Density functional theory calculations were carried out using the VASP code. We used the projector augmented wave (PAW) method to account for the core electrons, with the 6s and 5d electrons of Ir and the 2s and 2p electrons of C explicitly included in the valence. Single particle orbitals were expanded in plane-waves using a kinetic energy cutoff of 400 eV. Surfaces were modeled with the usual slab geometry, using a (9×9) supercell with four layers, of which the bottom two were kept frozen at the bulk interatomic distances. The vacuum was ∼17.5 Å for the clean surface and ∼15 Å for the system with the coronene molecule adsorbed on the surface. We used the gamma point only to sample the Brillouin zone. Energy barrier were estimated with the climbing-image nudged elastic band method,[14] using up to 11 images. Core-level binding energies were estimated within the final state approximation, where the screening from valence electrons is included, thus providing an accurate estimate of its effects on the core-level binding energies. According to previous theoretical studies,[15] the method used in our work calculates the core-level shifts with an accuracy better than 50 meV.

RESULTS AND DISCUSSION

Coronene was adsorbed on the surface at room temperature, T = 300 K. First, we performed NEXAFS measurements to address the issue of intact adsorbed molecule orientation with respect to the surface plane. Figure 1a reports the C K-edge absorption spectra measured at two different incident angles for submonolayer coverage. The most noticeable result is the strongly reduced intensity of the π^* resonance components at 286 eV when the electric field vector is almost parallel to the surface (normal incidence, NI), originating from the C 1s → LUMO electronic transitions,[16] and the increased spectral weight at about 292 eV due to the transition to the σ^* orbitals, thus indicating a nearly flat adsorption geometry. The presence of a shoulder extending up to about 288 eV can be explained, beside the C 1s → LUMO+1, +2, +3, and +4 π^* transitions, as due to the interaction of the molecules with the substrate. The strong modification in the electronic structure of coronene upon adsorption is confirmed by the UPS results reported in Figure 1b. These valence band (VB) spectra have been measured at normal emission ($h\nu$ = 34 eV) after different surface preparations. The spectrum acquired after deposition of a monolayer of coronene on clean Ir(111) (1, red), shows several peaks attributed to molecular signals, since they appear at different binding energies with respect to those present in the spectrum of clean Ir(111) (2, gray), which is dominated by the large d-band density of states. These molecular states can be associated with nondispersing features in the ARPES maps (see Supporting Information, Figure S1). In particular the M1 peak, at 1.8 eV, together with the next state (M2) appearing at 2.4 eV can be attributed to hybridization of the coronene molecular orbitals with the Ir 5d bands. The Ir(111) surface's ability in creating strong π bonds to PAHs is confirmed by considering the spectral components appearing for other coronene-based interfaces with weaker interactions, i.e. coronene multilayers grown on Ir(111) (3, black) and for coronene on graphene/Ir(111) (4, blue). In these cases, besides the rigid shift induced by different charge transfer, the VB spectra are a clear fingerprint of the coronene molecular orbitals (E_{2u}, B_{1g}, B_{2g}, E_{1g}, E_{2u}, A_{2u}, E_{2g}), whose BE distribution is in excellent agreement with previous experimental findings and theoretical calculations.[17−19] Further insight into the modification of the

DOI: 10.1021/jacs.5b12504
J. Am. Chem. Soc. 2016, 138, 3395−3402

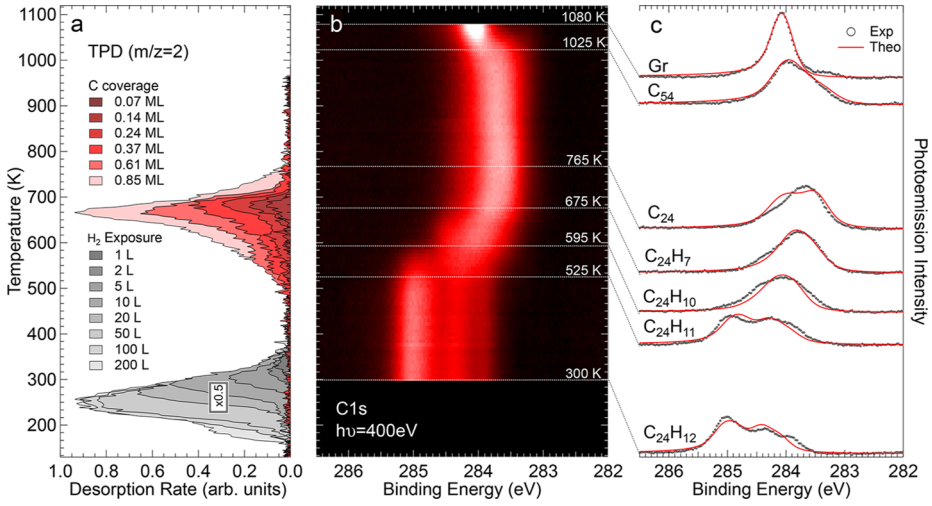

Figure 3. (a) Temperature-programmed desorption spectra (red scale) of m/z = 2 after coronene deposition at different coverages and T = 300 K. For comparison, desorption spectra (gray scale) corresponding to m/z = 2 after molecular hydrogen adsorption at T = 100 K are reported (intensity rescaled by a factor 0.5). (b) Temperature-dependent C 1s core-level spectra (about 100 spectra) shown as a two-dimensional intensity plot. (c) Comparison between selected experimental C 1s core-level spectra and fit results (red curves).

electronic structure due to adsorption was gained by high-resolution XPS C 1s core-level spectra, acquired at different molecular coverages (see Figure 1c). The three-peak spectral shape and binding energies are very different from those measured for coronene on graphene (blue curve), and for coronene in the gas phase, that displays a two-peak line shape.[16] In addition, the C 1s spectra measured at different coverages show the same line shape regardless of the coronene amount, suggesting that the adsorption configuration and site are not modified by intermolecular interactions in denser molecular layers or by the presence of surface defects, such as steps. It should be noted that the presence of three components cannot be simply justified as due to the geometrically nonequivalent carbon atoms in the molecule, i.e., those forming the inner hexagon, the middle one, and the outer ring, because the spectral weight does not match the 1:1:2 ratio corresponding to the population of such nonequivalent C atoms. The LEED pattern (see inset Figure 1c) does not show any additional diffraction spots, besides those arising from the hexagonal symmetry of the Ir substrate, indicating that the coronene molecules do not pack forming a long-range ordered layer, but are rather randomly distributed among the free adsorption sites.

In order to further shed light on the coronene adsorption geometry, and on the origin of the different core-level components, we performed DFT calculations. Several configurations were probed (see Supporting Information, Figure S2), including molecules with symmetry axes oriented along different directions, with different matches with respect to the high-symmetry adsorption sites of the Ir(111) surface, and also in nonplanar configurations. The minimum energy configuration corresponds to coronene adsorbed with the inner C hexagon in bridge-site and the molecular axis aligned parallel to the [101] direction of Ir(111) (see Figure 2c). The molecules assume a bowl-like shape (side view shown in Figure 2b), usually associated with π-conjugated compounds known as buckybowls or π-bowls.[20,21] These species have been found to commonly form stable adlayers on metal surfaces, as in the case of corannulene ($C_{20}H_{10}$) on Cu(110)[22,23] and of sumanene ($C_{21}H_{12}$) on Ag(111).[24] In our case, the adsorbed molecule develops its bowl opening upward: C atoms in the inner ring are about 0.23 Å closer to the surface with respect to C atoms in the outer ring (see Figure 2a). The bowl-shaped geometry is enhanced by the hydrogen atoms displaying an average height of 2.74 Å, 0.7 Å farther from the surface than the inner C atoms, and a C−H bond angle ranging from 22° to 39° with respect to the Ir surface plane. In order to test the consistency of the minimum energy adsorption structure we compared in Figure 2d the experimental C 1s core-level spectra (empty circles), for which the molecule−substrate interaction is expected to have a strong influence, and fit results (solid line). We computed the C 1s core-level binding energy (BE) for each of the 24 C atoms of the coronene molecules, including also final state effects due to core-hole screening. The results, illustrated in Figure 2d, show that the computed BEs for the carbon atoms in the coronene molecule are not only linked to some extent to the carbon−metal distance (C atoms in the central ring showing the highest BEs), but are strongly dependent on the positions with respect to the first-layer Ir atoms. This is especially true for those C atoms sitting in the outer ring and bonded to H atoms, whose C 1s BE depends on the degree of interaction with the substrate Ir atoms, besides the bond with H instead of another C. The good agreement between experimental data and fit results strongly supports the DFT calculated molecular adsorption geometry.

In order to explore the mechanism of coronene dissociation we initially employed TPD, in the temperature range 150−590 K (see Figure 3a), with the aim of finding the threshold of hydrogen desorption (mass to charge ratio m/z = 2), which can be used as a fingerprint for C−H breakup. Desorption spectra corresponding to different initial coverages of coronene are reported in red colored scale, indicating that H_2 in gas phase can be detected only above 500 K, with a maximum desorption rate at temperatures slightly higher than 650 K. To verify that on coronene the process of C−H bond dissociation does not take place at lower temperature, we compared the TPD data with a similar H_2 desorption experiment starting from hydrogen adsorption at T = 100 K. It is known that H_2 adsorbs dissociatively on Ir(111)[25,26] and that the onset of desorption is indicative of the recombination of two H atoms after surface diffusion. The large difference in H_2 formation temperature,

DOI: 10.1021/jacs.5b12504
J. Am. Chem. Soc. 2016, 138, 3395−3402

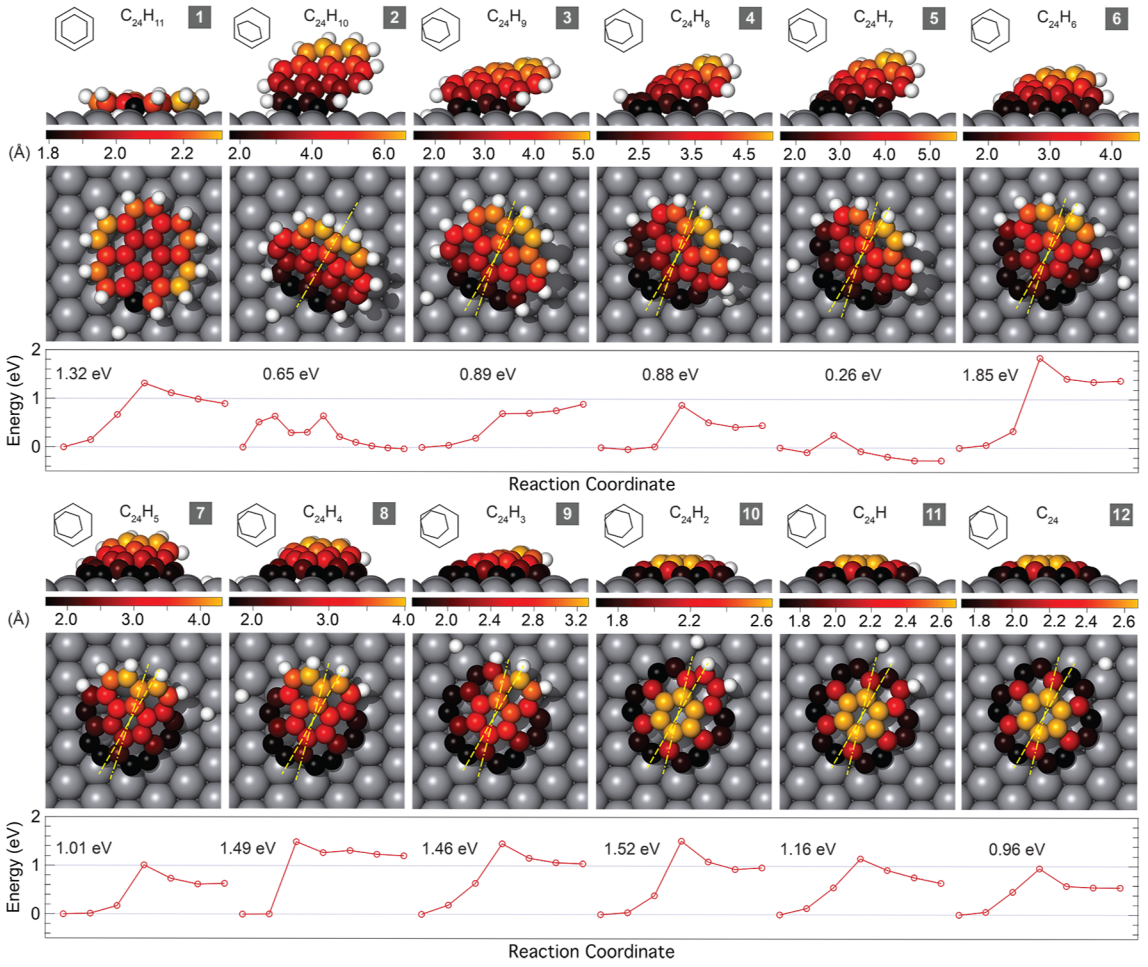

Figure 4. (a) Illustration of final states side and top views of $C_{24}H_n$ through the 12 sequential C−H bond cleavages that bring coronene molecules to the nanodome configuration. Different colors correspond to different carbon−metal substrate heights. The colors have been rescaled in each step to emphasize the geometrical differences in each configuration (the height scale in Å is also reported for each step of the reaction). Above each illustration, a schematic representation of the coronene to Ir relative orientation is reported. The yellow dash-dotted line in step 2 represents the symmetry axis shared by the adsorbed coronene molecule and the Ir substrate. In steps n = 3−12, the dashed line represents the original coronene orientation, while the dash-dotted line represents the current one. Below each illustration, a graph representing the energy evolution during the NEB simulations is shown with the total energy barrier for the single dehydrogenation step.

and the lack of any overlap on the temperature scale of the desorption spectra from H_2 and $C_{24}H_{12}$, is a clear proof that coronene molecules undergo the first C−H breakup only above 500 K. Further information about the coronene dissociation process was obtained following *in situ* the temperature evolution of the C 1s core-level spectrum from RT to 1120 K. The combination of a high-efficiency electron energy analyzer with a homemade delay-line detection system allowed us to measure each photoemission spectrum in about 30 s (still keeping the overall energy resolution to 40 meV), providing real-time spectroscopic visualization of the intermediate reaction stages. The image plot in Figure 3b shows the evolution of the C 1s spectrum at increasing temperature. As expected, the spectrum does not change during the initial stage of the temperature ramp (0.25 K/s), and only above 525 K, the onset temperature for H_2 desorption in the TPD spectra, clear changes are observed. The spectral intensity shifts to lower BE, reaching a rather constant value above 700 K, when the TPD results show that all hydrogen atoms have desorbed. Only above 1000 K the C 1s signal starts shifting back to higher BE. The BE value of 284.10 eV, reached above 1050 K, is a clear fingerprint of high-temperature graphene formation.[27−30]

Notably, during the dissociation process, there is no loss in the overall C 1s spectral intensity, indicating that the energy barrier for C−H bond cleavage is lower than that for desorption of the intact molecule or C containing species. Unambiguous chemical assignment of the experimentally observed C 1s core-level line shape is, however, not easy, due to the high number of possible configurations of the dehydrogenated transient products. In order to interpret the C 1s spectral sequence, and to reach an atomistic understanding of the transient states involved in the thermal breakup of coronene, we resorted to DFT by performing extensive calculations of the energy barriers between the computed intermediate species, using the nudged elastic band (NEB) method.[14]

In Figure 4, we show the 12 molecule−substrate configurations corresponding to the energetically most favored reaction pathway for breaking each C−H bond in n sequential steps (with n from 1 to 12), leaving the dehydrogenated molecules and an additional single H atom on the surface. The reaction-coordinate energy diagrams reported under the geometrical configurations are given with respect to the energy of the n − 1 configuration, n = 0 being the intact adsorbed coronene molecule. It is important to stress that, despite the

DOI: 10.1021/jacs.5b12504
J. Am. Chem. Soc. 2016, 138, 3395−3402

higher final state energy of each dehydrogenation step, the overall reaction can easily proceed at the temperature of our experiments, as dissociated H atoms can diffuse very rapidly on the surface forming H_2, which desorbs and is not available for the reverse process. For this reason the final state of structure n does not exactly correspond to the initial state of structure $n + 1$, where a H atom has been removed. What is intriguing in our findings is the complex evolution of the molecular geometry during the dehydrogenation steps. Close inspection of the images shown in Figure 4 (see also movie in the Supporting Information) indicates that the stepwise dehydrogenation mechanism appears to be driven by the proximity of the C outer ring atom to the final adsorption position. At the beginning, the intact adsorbed molecule has significant internal C−C strain with respect to the gas phase configuration (see Supporting Information, Figure S3). The peripheral C closest to the most favorable position is the one which will lose an H atom in the next reaction step; the dissociation begins (see Figure 4, $n = 1$) from one of the four equivalent peripheral C atoms closest to the top position, which, after losing its H atom, binds strongly to the surface and approaches its preferred adsorption site, much closer to the surface. The next key step of the dissociation, during the second dehydrogenation ($n = 2$), corresponds to the abrupt molecular lifting from the surface, resulting in an almost complete internal strain relief (see Supporting Information, Figure S3). In fact, three peripheral C atoms are positioned in equivalently favorable sites, giving therefore three candidate C−H bonds for the next dehydrogenation. But the lifting of the molecule has been found to give an energy gain of 0.67 eV with respect to the other configurations, thereby losing one of the two symmetry axes in the molecule, and causing the candidate C−H bond closest to the previously dehydrogenated one to be broken. At this point, one symmetry axis of the molecule with respect to the substrate still remains. Always keeping in mind that the driving mechanism for dehydrogenation is the proximity of the peripheral C atom to a top site, the two C atoms, adjacent to the freshly dehydrogenated carbons, are found to be equivalent. The evolution of the system toward the $n = 3$ state results in a clear twist of the molecule in one direction, in order to better accommodate the newly dehydrogenated C atom in its favored bond site on the substrate. This causes the loss of the second symmetry axis, and the remaining evolution of the dissociation reaction is fully determined. It is significant that during the dehydrogenation process also the atoms of the Ir substrate are slightly rearranged, in particular becoming more elevated with respect to the average surface plane, which eventually contributes to the formation of a stronger molecule−Ir bond. From this step on, the molecule evolves by gradually completing the rotation to the final adsorption geometry, and by curling toward a dome shape configuration, always losing H atoms next to dehydrogenated bonds. This gradually changing shape increases the internal strain of the part attached to the substrate, while always keeping one end lifted until the very end, allowing for some strain to be relieved in the lifted portion of the molecule during the intermediate steps. The topology during the dissociation process is also affected by the contributions of the σ and π orbital overlap with the substrate d-bands, the former tending to cause the C rings to stand perpendicular to the surface, the latter trying to push the C ring parallel to it. The final state configuration is very similar to what has been found for the initial stages of growth of graphene using ethylene: dome-shaped C nanoislands whose interactions with the Ir substrate take place only at the cluster edges.[28] With increasing temperature, the mobility of the nanodomes becomes large enough to permit the formation of larger clusters and eventually graphene.[31]

In order to confirm that the reaction intermediates, including the molecular lifting, twisting and curling, are more favorable with respect to the flat behavior, we simulated the C 1s core-level spectra for all the carbon atoms in the most important configurations in Figure 4 (1, 2, 5, 11, and 12), as well as for coronene, a larger nanodome formed by 54 C atoms (C_{54}) and graphene. The fit results, reported in Figure 3c along with the experimental data, show an excellent agreement: the three-component line shape, associated with the $C_{24}H_{12}$ and $C_{24}H_{11}$ molecules, at 525 K changes and shifts to lower BE, and only when larger nanodomes are formed, because of coalescence and nucleation (see fit result corresponding to C_{54}), the spectral intensity distribution gets narrower. The single peak at 284.1 eV, fingerprint of graphene formation on Ir(111), appears only at high temperature (1080 K). We want to stress that the sequential dehydrogenation is a statistical process, and during the annealing there could be several different $C_{24}H_n$ species present on the surface. The amount of each species depends, besides from the energy barrier, also on pre-exponential factors and diffusion constants among other factors, which are difficult to calculate. In Figure 3c, we report the C 1s core-level spectra, along with the single molecular species fit result, for the most important intermediate molecules. Beside the initial and final configurations, corresponding to coronene and the C_{24} nanodome respectively, we report the spectrum associated with $C_{24}H_7$, which has the highest dehydrogenation barrier and is therefore expected to be stable for a larger temperature window on the surface. We also show the fit result associated with the tilted molecule, $C_{24}H_{10}$, since it represents a crucial step in the dissociation pathway, and to $C_{24}H_{11}$, which represents the first dissociation product. Even though the process illustrated in Figure 4 is the most energetically favorable, we also tested many other reaction paths that revealed striking differences in terms of geometry, and do not include the process of molecular lifting and curling. For example we found that an alternative possibility is that, after the first dehydrogenation, the molecules break the next C−H bond but still remain flat on the surface. However, the final state is 0.67 eV higher in energy. Moreover, the evolution of the reaction following this new sequence would end up with a C_{24} carbon cluster in a geometrical configuration that is by far not energetically favorable. In fact, it is important to stress that the unrotated C cluster, i.e., the one presenting the same azimuthal orientation as the original coronene molecule, has a 2.27 eV higher energy. Notably, the reaction path involving the flat dissociation behavior results in a calculated C 1s core-level spectrum with an additional component growing at lower BE (at 282.9 eV), which is not experimentally observed. In fact, during the flat dissociation pathway, some Ir atoms that bind to peripheral C atoms of the partially dissociated molecule, are also bound to another C atom. This produces the theoretically predicted, but not experimentally observed, low BE component in the C 1s spectrum. As a final step of our investigation, we have compared the experimental $C_{24}H_{12}$ coverage evolution with temperature, as extracted from the C 1s photoemission data (see Supporting Information, Figure S4), to a theoretical prediction based on a microkinetic model, assuming that the reaction rate depends on the activation energy of the first C−H bond-breaking reaction step through a Boltzmann factor, with

DOI: 10.1021/jacs.5b12504
J. Am. Chem. Soc. 2016, 138, 3395−3402

an energy barrier deduced from the NEB calculations, allowing only the pre-exponential order of magnitude as a free parameter. The temperature behavior is in good agreement with the experimentally observed decrease of the $C_{24}H_{12}$ population when the pre-exponential factor is equal to 10^{10}. This value, that at first instance seems quite low if compared with the typical value of 10^{13}, is however not surprising. As recently reported by Campbell et al. by discussing extensive experimental results,[32] ν_{diss} prefactors for dissociation are found typically 1/10 to $1/10^5$ of the prefactors for desorption ν_{des} of the same molecule, with an average ratio (ν_{diss}/ν_{des}) of about 1/1000, because of entropy loss at the transition state. It is interesting to compare our experimental finding with those obtained for the simplest aromatic molecule, i.e. benzene (C_6H_6).[33] Theoretical calculations of benzene adsorption on Cu(100) show that, after the first hydrogen scission starting from its flat adsorption configuration, also the phenyl radical C_6H_5 and the ortho-benzyne species C_6H_4 assume upright configurations. It is interesting to observe that instead, the dissociation of benzene on Pt(111), which is a transition metal quite similar to Ir, results in a tilted configuration with the C atoms adsorbed through C at the top site.[34] Our results therefore suggest that the process of thermally activated molecular lifting can be a more general behavior in the dissociation process of similar molecules, also for larger PAHs. We suppose that this is the case for other transition metal surfaces, where the presence of unsaturated C bonds could lead to the development of strong interactions between the partially dehydrogenated molecules and the metal substrates. The main driving force resulting in the tilt and rotation of the molecule before curling, i.e., the creation of new bonds with the substrate which breaks the molecular symmetries and allows for some internal strain relief, somehow mimics what happens in the case of heterocyclic aromatic adsorbates such as pyridine, pyrrole, and thiopene for which, besides flat-lying configurations, also tilted geometries have been reported.[35]

CONCLUSIONS

We have shown, using a multimethod experimental approach and extensive theoretical calculations, that coronene molecules adsorbed on Ir(111) undergo major conformational changes during the dissociation process, which bring the molecules from a flat, slightly upward-pointing bowl shape to graphene through a series of exotic configurations. Upon the second C−H bond cleavage, the molecules tilt upward with respect to the surface, and then rotate to accommodate the reactive C terminations to the most favorable bond site with the substrate. During the lifting, the C−C strain is initially relieved, while as the dehydrogenation proceeds, the molecules experience a progressive increase in the average interatomic distance, and gradually settle to form peculiar dome shaped nanographene flakes. By exploiting this reaction mechanism, we envisage the possibility of creating new nanostructures with different functionalities by encapsulating single adatoms below the carbon dome, through diffusion of the new species underneath the carbon disk just before the formation of large carbon clusters, in a similar way as already demonstrated for larger Sn nanoparticles for applications in lithium batteries.[36] It is clear that this concept would require an accurate control of the status of the molecular structure, which is a challenging task, but the lifting of the molecule could be an important step to follow this strategy. In fact, the process of intercalation of atomic species below already formed nanographenes, which could have interesting application in spintronics[37] and energy storage,[38] is strongly hindered by the strong carbon−metal bonds formed at the edges which prevent the atomic penetration below the C flake. Besides the confinement of magnetic species below nanographene flakes, also the presence of chemically inert species below the nanographenes is expected to modify the electronic edge states giving rise to interesting magnetic phenomena.[39] The use of nanostructured surfaces, such as those formed by a high density of monoatomic steps or vacancies, could be a possibility to reduce the geometrical degree of freedom forced by the hexagonal surface of Ir(111), with C_{3v} symmetry, and achieve an easier control of the reaction parameters. Finally, the control of molecular tilt in PAHs could tailor their chemical reactivity, by activating or inhibiting specific reactions that are usually catalyzed by the surface, as reported, for example, in the case of different carbonyl compounds, more specifically aldehydes, on transition metal substrates.[40,41]

ASSOCIATED CONTENT

Supporting Information

The Supporting Information is available free of charge on the ACS Publications website at DOI: 10.1021/jacs.5b12504.

Angle-resolved photoemission data, additional DFT-calculated adsorption configurations, C−C bond length histograms, and microkinetic reaction model (PDF)

Movie showing the structural changes of the coronene molecule during the dehydrogenation process as obtained by the Nudged Elastic Band calculations (MPG)

AUTHOR INFORMATION

Corresponding Author

*alessandro.baraldi@elettra.eu

Author Contributions

#D.C. and L.O. contributed equally to this work.

Notes

The authors declare no competing financial interest.

ACKNOWLEDGMENTS

We acknowledge financial support from MIUR through the project PRIN entitled "GRAF. Frontiers in graphene research: understanding and controlling advanced functionalities" (No. 20105ZZYSE001) and from the University of Trieste through the program "Finanziamento di Ateneo per progetti di ricerca scientifica - FRA 2014". N.J. acknowledges support from the International Centre for Theoretical Physics (ICTP) under the "Programme for Training and Research in Italian Laboratories" (TRIL). This work used the ARCHER UK National Supercomputing Service (http://www.archer.ac.uk). This research also used resources of the Oak Ridge Leadership Computing Facility, which is a U.S. DOE Office of Science User Facility supported under Contract DE-AC05-00OR22725

REFERENCES

(1) Otero, G.; Biddau, G.; Sanchez-Sanchez, C.; Caillard, R.; Lopez, M. F.; Rogero, C.; Palomares, F. J.; Cabello, N.; Basanta, M. A.; Ortega, J.; Mendez, J.; Echavarren, A. M.; Perez, R.; Gomez-Lor, B.; Martin-Gago, J. A. *Nature* **2008**, *454*, 865−868.

(2) Cai, J.; Ruffieux, P.; Jaafar, R.; Bieri, M.; Braun, T.; Blankenburg, S.; Muoth, M.; Seitsonen, A. P.; Saleh, M.; Feng, X.; Müllen, K.; Fasel, R. *Nature* **2010**, *466*, 470−473.

DOI: 10.1021/jacs.5b12504
J. Am. Chem. Soc. 2016, 138, 3395−3402

(3) Müllen, K.; Rabe, J. P. *Acc. Chem. Res.* **2008**, *41*, 511−520.
(4) Narita, A.; Wang, X.-Y.; Feng, X.; Müllen, K. *Chem. Soc. Rev.* **2015**, *44*, 6616−6643.
(5) Son, Y.-W.; Cohen, M. L.; Louie, S. G. *Nature* **2006**, *444*, 347−349.
(6) Yang, L.; Park, C.-H.; Son, Y.-W.; Cohen, M. L.; Louie, S. G. *Phys. Rev. Lett.* **2007**, *99*, 186801.
(7) Chen, Y.-C.; de Oteyza, D. G.; Pedramrazi, Z.; Chen, C.; Fischer, F. R.; Crommie, M. F. *ACS Nano* **2013**, *7*, 6123−6128.
(8) Ruffieux, P.; Cai, J.; Plumb, N. C.; Patthey, L.; Prezzi, D.; Ferretti, A.; Molinari, E.; Feng, X.; Müllen, K.; Pignedoli, C. A.; Fasel, R. *ACS Nano* **2012**, *6*, 6930−6935.
(9) Fujii, S.; Enoki, T. *Acc. Chem. Res.* **2013**, *46*, 2202−2210.
(10) Narita, A.; Feng, X.; Müllen, K. *Chem. Rec.* **2015**, *15*, 295−309.
(11) Treier, M.; Pignedoli, C. A.; Laino, T.; Rieger, R.; Müllen, K.; Passerone, D.; Fasel, R. *Nat. Chem.* **2011**, *3*, 61−67.
(12) Baraldi, A.; Comelli, G.; Lizzit, S.; Cocco, D.; Paolucci, G.; Rosei, R. *Surf. Sci.* **1996**, *367*, L67−L72.
(13) Doniach, S.; Šunjić, M. *J. Phys. C: Solid State Phys.* **1970**, *3*, 285.
(14) Henkelman, G.; Uberuaga, B. P.; Jónsson, H. *J. Chem. Phys.* **2000**, *113*, 9901−9904.
(15) Köhler, L.; Kresse, G. *Phys. Rev. B: Condens. Matter Mater. Phys.* **2004**, *70*, 165405(1−9).
(16) Fronzoni, G.; Baseggio, O.; Stener, M.; Hua, W.; Tian, G.; Luo, Y.; Apicella, B.; Alfé, M.; de Simone, M.; Kivimäki, A.; Coreno, M. *J. Chem. Phys.* **2014**, *141*, 044313.
(17) Boschi, R.; Clar, E.; Schmidt, W. *J. Chem. Phys.* **1974**, *60*, 4406−4418.
(18) Schroeder, P. G.; France, C. B.; Parkinson, B. A.; Schlaf, R. *J. Appl. Phys.* **2002**, *91*, 9095−9107.
(19) Medjanik, K.; Kutnyakhov, D.; Nepijko, S. A.; Schonhense, G.; Naghavi, S.; Alijani, V.; Felser, C.; Koch, N.; Rieger, R.; Baumgarten, M.; Müllen, K. *Phys. Chem. Chem. Phys.* **2010**, *12*, 7184−7193.
(20) Wu, Y.-T.; Siegel, J. S. *Chem. Rev.* **2006**, *106*, 4843−4867.
(21) Tsefrikas, V. M.; Scott, L. T. *Chem. Rev.* **2006**, *106*, 4868−4884.
(22) Parschau, M.; Fasel, R.; Ernst, K.-H.; Gröning, O.; Brandenberger, L.; Schillinger, R.; Greber, T.; Seitsonen, A.; Wu, Y.-T.; Siegel, J. *Angew. Chem., Int. Ed.* **2007**, *46*, 8258−8261.
(23) Xiao, W.; Passerone, D.; Ruffieux, P.; Aït-Mansour, K.; Gröning, O.; Tosatti, E.; Siegel, J. S.; Fasel, R. *J. Am. Chem. Soc.* **2008**, *130*, 4767−4771.
(24) Jaafar, R.; Pignedoli, C. A.; Bussi, G.; Aït-Mansour, K.; Groening, O.; Amaya, T.; Hirao, T.; Fasel, R.; Ruffieux, P. *J. Am. Chem. Soc.* **2014**, *136*, 13666−13671.
(25) Hagedorn, C. J.; Weiss, M. J.; Weinberg, W. H. *Phys. Rev. B: Condens. Matter Mater. Phys.* **1999**, *60*, R14016−R14018.
(26) Moritani, K.; Okada, M.; Nakamura, M.; Kasai, T.; Murata, Y. *J. Chem. Phys.* **2001**, *115*, 9947−9959.
(27) Preobrajenski, A. B.; Ng, M. L.; Vinogradov, A. S.; Mårtensson, N. *Phys. Rev. B: Condens. Matter Mater. Phys.* **2008**, *78*, 073401.
(28) Lacovig, P.; Pozzo, M.; Alfè, D.; Vilmercati, P.; Baraldi, A.; Lizzit, S. *Phys. Rev. Lett.* **2009**, *103*, 166101.
(29) Lizzit, S.; Baraldi, A. *Catal. Today* **2010**, *154*, 68−74.
(30) Presel, F.; Jabeen, N.; Pozzo, M.; Curcio, D.; Omiciuolo, L.; Lacovig, P.; Lizzit, S.; Alfè, D.; Baraldi, A. *Carbon* **2015**, *93*, 187−198.
(31) Coraux, J.; N'Diaye, A. T.; Engler, M.; Busse, C.; Wall, D.; Buckanie, N.; zu Heringdorf, F.-J. M.; van Gastel, R.; Poelsema, B.; Michely, T. *New J. Phys.* **2009**, *11*, 023006.
(32) Campbell, C. T.; Árnadóttir, L.; Sellers, J. R. *Z. Phys. Chem.* **2013**, *227*, 1435−1454.
(33) Lesnard, H.; Bocquet, M.-L.; Lorente, N. *J. Am. Chem. Soc.* **2007**, *129*, 4298−4305.
(34) Gao, W.; Zheng, W. T.; Jiang, Q. *J. Chem. Phys.* **2008**, *129*, 164705.
(35) Jenkins, S. J. *Proc. R. Soc. London, Ser. A* **2009**, *465*, 2949−2976.
(36) Cui, G.; Hu, Y.-S.; Zhi, L.; Wu, D.; Lieberwirth, I.; Maier, J.; Müllen, K. *Small* **2007**, *3*, 2066−2069.
(37) Sicot, M.; Leicht, P.; Zusan, A.; Bouvron, S.; Zander, O.; Weser, M.; Dedkov, Y. S.; Horn, K.; Fonin, M. *ACS Nano* **2012**, *6*, 151−158.
(38) Xu, F.; Tang, Z.; Huang, S.; Chen, L.; Liang, Y.; Mai, W.; Zhong, H.; Fu, R.; Wu, D. *Nat. Commun.* **2015**, *6*, 7221.
(39) Fujii, S.; Ziatdinov, M.; Ohtsuka, M.; Kusakabe, K.; Kiguchi, M.; Enoki, T. *Faraday Discuss.* **2014**, *173*, 173−199.
(40) Chiu, M. E.; Watson, D. J.; Kyriakou, G.; Tikhov, M. S.; Lambert, R. M. *Angew. Chem.* **2006**, *118*, 7692−7696.
(41) Brandt, K.; Chiu, M. E.; Watson, D. J.; Tikhov, M. S.; Lambert, R. M. *J. Am. Chem. Soc.* **2009**, *131*, 17286−17290.

DOI: 10.1021/jacs.5b12504
J. Am. Chem. Soc. 2016, 138, 3395−3402